Published in final edited form as:

NMR Biomed. 2015 December ; 28(12): 1645–1654. doi:10.1002/nbm.3412.

Intravoxel Incoherent Motion Imaging Kinetics during Chemoradiotherapy for Human Papillomavirus-Associated Squamous Cell Carcinoma of the Oropharynx: Preliminary Results from a Prospective Pilot Study

Yao Ding, PhD[1,2], **John D. Hazle, PhD**[2], **Abdallah S. R. Mohamed, MD, MSc**[1,7], **Steven J. Frank, MD**[1], **Brian P. Hobbs, PhD**[3], **Rivka R. Colen, MD**[4], **G. Brandon Gunn, MD**[1], **Jihong Wang, PhD**[5], **Jayashree Kalpathy-Cramer, PhD**[8], **Adam S. Garden, MD**[1], **Stephen Y. Lai, MD, PhD**[6], **David I. Rosenthal, MD**[1], and **Clifton D. Fuller, MD, PhD.**[1,9]

[1]Department of Radiation Oncology, The University of Texas MD Anderson Cancer Center, Houston, Texas, USA

[2]Department of Imaging physics, The University of Texas MD Anderson Cancer Center, Houston, Texas, USA

[3]Department of Biostatistics, The University of Texas MD Anderson Cancer Center, Houston, Texas, USA

[4]Department of Radiology, The University of Texas MD Anderson Cancer Center, Houston, Texas, USA

[5]Department of Radiation Physics, The University of Texas MD Anderson Cancer Center, Houston, Texas, USA

[6]Department of Head and Neck Surgery, The University of Texas MD Anderson Cancer Center, Houston, Texas, USA

[7]Department of Clinical Oncology and Nuclear Medicine, Faculty of Medicine, University of Alexandria, Alexandria, Egypt

[8]Athinoula A. Martinos Center for Biomedical Imaging, Massachusetts General Hospital/Division of Health Sciences & Technology, Massachusetts Institute of Technology, Charlestown, MA, USA

Address correspondence to Clifton David Fuller, MD, PhD, Department of Radiation Oncology, Unit 0097, The University of Texas MD Anderson Cancer Center, 1515 Holcombe Blvd., Houston, TX 77030, USA, Phone: 713-563-2300, Fax: 713-563-2366, cdfuller@mdanderson.org. AND Abdallah S. R. Mohamed, MD, MSc, Department of Radiation Oncology, Unit 0097, The University of Texas MD Anderson Cancer Center, 1515 Holcombe Blvd., Houston, TX 77030, USA, Phone: 832-955-7920, Fax: 713-563-2366, asmohamed@mdanderson.org.

Disclosures of Conflicts of Interest: Y.D. was partially supported by an MD Anderson Institutional Research Grant Program award and the Bernard W. Biedenharn Foundation. A.S.R.M. received salary support from the Union for International Cancer Control/ American Cancer Society International Fellowships for Beginning Investigators. C.D.F. received support from the National Institutes of Health/National Cancer Institute's Paul Calabresi Clinical Oncology Award Program (K12 CA088084-06) and Clinician Scientist Loan Repayment Program (L30 CA136381-02); the SWOG/Hope Foundation's Dr. Charles A. Coltman, Jr., Fellowship in Clinical Trials; a Center for Advanced Biomedical Imaging/General Electric Healthcare In-Kind Award; a Center for Advanced Biomedical Imaging and Center for Radiation Oncology Research of The University of Texas MD Anderson Cancer Center Technology Development Grant; and an Elekta AB/MD Anderson Cancer Center Department of Radiation Oncology Seed Grant. This work was supported in part by the National Institutes of Health/National Cancer Institute under award number P30CA016672. These funders/ supporters played no role in the study design; collection, analysis, or interpretation of data; manuscript writing; or decision to submit the report for publication.

[9]The University of Texas Graduate School of Biomedical Sciences, Houston, TX, USA

Abstract

This study aims to identify the temporal kinetics of intravoxel incoherent motion (IVIM) magnetic resonance imaging (MRI) in patients with human papillomavirus-associated (HPV+) oropharyngeal squamous cell carcinoma. Patients were enrolled under an IRB-approved protocol as part of ongoing prospective clinical trial. All patients underwent two MRI studies, a baseline scan before chemoradiotherapy and a midtreatment scan 3–4 weeks of treatment initiation. Parametric maps representing pure diffusion coefficient (D), pseudo-diffusion coefficient (D*), perfusion fraction (*f*), and apparent diffusion coefficient (ADC) were generated. The Mann-Whitney U test was used to assess temporal variation of IVIM metrics. Bayesian quadratic discriminant analysis (QDA) was used to evaluate the extent to which midtreatment changes in IVIM metrics could be combined to predict sites that would achieve complete response (CR) in multivariate analysis. A total of 31 patients were included in the final analysis with 59 lesions. Pretreatment ADC and D values of the complete response (CR) lesions (n=19) were significantly lower than non-CR lesions (n=33). Midtreatment ADC, D, and *f* values were significantly higher ($P < .0001$) than pretreatment values for all lesions. Each increase in normalized ΔADC of size 0.1 yielded a 1.45-fold increase in the odds of CR ($P<.0003$), each increase in normalized ΔD of size 0.1 yielded a 1.53-fold increase in the odds of CR ($P<.0002$), and each unit increase in Δ*f* yielded a 2.29-fold increase in the odds of CR ($P < .02$). Combined ΔD and ΔADC were integrated into a multivariate prediction model and attained an AUC=0.87 (95% CI: 0.79, 0.96) as well as sensitivity=0.63, specificity=0.85, and accuracy=0.78 under leave-one-out cross-validation. In conclusion, IVIM is feasible and potentially useful in prediction and assessment of early response of HPV+ oropharyngeal squamous cell carcinoma to chemoradiotherapy.

Graphical abstract

Our data showed that a low pretreatment apparent diffusion coefficient (ADC) and pure diffusion coefficient (D) values were associated with early radiologic CR during chemoradiotherapy. Midtreatment ADC, D, and *f* values were significantly higher ($P < .0001$) than pretreatment values for all lesions. A model combining ΔADC and ΔD is highly predictive of early CR. Noninvasive IVIM MRI is feasible and potentially useful for predicting and assessing early responses of HPV+ oropharyngeal SCC to chemoradiotherapy.

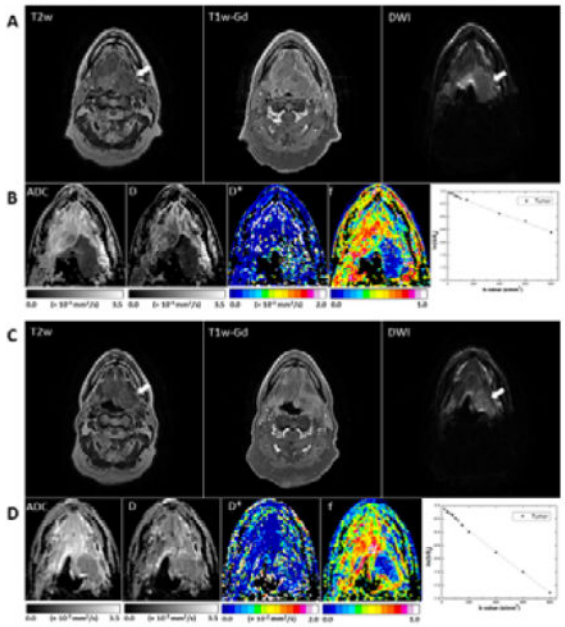

Keywords

Intravoxel incoherent motion imaging; HPV-associated oropharyngeal cancer; Chemoradiotherapy; Response assessment

Introduction

Head and neck squamous cell carcinoma (HNSCC) has an estimated incidence of approximately 50,000 annual cases in the United States, with an annual mortality estimated at 11,400 persons. Even with the use of chemotherapy concurrently with radiation, local failures predominate as a failure pattern (1,2). Opportunities for radiation dose escalation and therapeutic intensification are limited because of the risk of damage to adjacent normal tissues in the beam path. Ideally, personalized adaptive therapy would allow dose escalation/de-escalation at the individual, rather than population, level, based on imaging biomarkers which portend therapeutic response (3,4). If a probable outcome can be predicted before or at an early stage of treatment, a patient could be spared ineffective and unnecessary toxicity through treatment deintensification or dose modification. Magnetic resonance imaging (MRI) techniques, including proton spectroscopy, diffusion-weighted imaging (DWI), and dynamic contrast-enhanced imaging, have been proposed as such noninvasive imaging biomarkers for prediction and early detection of response to cancer therapy (5,6).

DW-MRI reflects the cell density of tissue and thus may indicate regions with a high tumor load(7). The apparent diffusion coefficient (ADC), the most common quantitative parameter in DW-MRI, reflects the microscopic diffusion of water molecules and is determined using a monoexponential approach. Recently, ADC has been used for prediction or early detection of treatment response in HNSCC (8–10). However, ADC values are influenced by both

tissue diffusivity and microvascular perfusion. In the mid-1980s, Le Bihan et al proposed the intravoxel incoherent motion (IVIM) model to separate the perfusion-related parameters (pseudo-diffusion coefficient D* and perfusion fraction *f*) and the diffusion-related parameter (pure diffusion coefficient D) by employing biexponential fitting analysis (11,12). Thus, IVIM MRI reflects not only cell density but also tissue microcapillary blood perfusion, which is correlated to tumor oxygenation(13). These properties affect radiation sensitivity.

The IVIM technique has been widely applied in studies of cancer in the brain (14,15), abdomen (liver, kidney, and pancreas) (16–18), and pelvis (prostate) (19). IVIM has also been used in the head and neck for predicting malignancy, cancer staging, detecting nodal metastases, and monitoring treatment response (20–24).

Recently, it has become apparent that human papillomavirus-associated (HPV+) oropharyngeal tumors exhibit a more radiosensitive phenotype than non-HPV head and neck cancers (25,26). While IVIM has been demonstrated to correlate with nodal response to therapy (27), no data on pre- and midtreatment parameter kinetics or the potential utility of IVIM for predicting response to chemoradiotherapy in a prospective uniform cohort of HPV + cancers have been presented. Furthermore, data suggest that midtreatment response (as measured by anatomic imaging (28,29) or DWI (10,30)) may serve as a reasonable surrogate for locoregional control in HNSCC.

In this study, we sought to (i) determine the feasibility of serial, standardized IVIM data acquisition as part of an ongoing prospective study of chemoradiotherapy for HPV+ oropharyngeal cancers, (ii) characterize tumor and nodal pre- and mid-chemoradiotherapy temporal kinetics of IVIM, and (iii) determine whether temporal changes in IVIM parameters during chemoradiotherapy are associated with early treatment response as measured by RECIST (Response Evaluation Criteria in Solid Tumors) assessment (31) of midtreatment imaging.

Materials and Methods

Patients

Patients diagnosed with HPV+ oropharyngeal SCC were included in this study under an Institutional Review Board (IRB)-approved protocol with study-specific informed consent as part of an ongoing prospective clinical trial (32). All patients were scanned between October 2013 and May 2015. The criteria for inclusion were age older than 18 years; histologically documented stage III or IV HPV+ SCC of the oropharynx, according to the American Joint Committee on Cancer (AJCC) staging criteria; eligibility for definitive chemoradiotherapy; and an Eastern Cooperative Oncology Group (ECOG) performance status of 0 to 2. Patients were excluded for any of the following reasons: definitive resection of primary tumor or administration of induction chemotherapy before radiotherapy; a prior cancer diagnosis, except appropriately treated localized epithelial skin cancer or cervical cancer; prior radiotherapy to the head and neck; contraindications to gadolinium-based contrast agents; or claustrophobia.

All patients underwent two MRI studies, a baseline scan within 1 week before starting chemoradiotherapy treatment and a midtreatment scan 3–4 weeks after treatment initiation. RECIST criteria (31) were utilized for categorical midtherapy tumor/node assessment. Midtreatment results were categorized as stable disease, partial response (PR), or complete response (CR) based on radiological (T1-weighted (T1w)-Gd MRI) assessments by an experienced head and neck radiologist (RRC) and two experienced radiation oncologists (ASRM, CDF). Additionally, all patients had complete physical exanimation, fibroptic endoscopy, MRI, and contrast-enhanced diagnostic CT or FDG PET-CT done 2–3 months after treatment completion to assess the final treatment response.

MRI Protocol

MRI examinations were performed using a previously published custom immobilization method (33) and a 3.0T Discovery 750 MRI scanner (GE Healthcare, Waukesha, WI) with laterally placed 6-element flex coils centered on the base of the tongue with immobilization devices (Klarity Medical Products, Newark, OH) (Fig. 1). Patient data were indexed to those obtained from pretreatment MRI done with the patient set up on a flat insert table (GE Healthcare) using the same immobilization devices as those used for daily image-guided therapy, including an individualized thermoplastic head and shoulder mask, a customized foam mold head support, and an intraoral tongue-immobilizing/swallow-suppressing dental stent. This standardized immobilization approach, demonstrated to improve image coregistration in longitudinal scans and reduce interval physiologic motion (e.g. swallowing) (33), was used for all patients.

Geometrical scan parameters (e.g. field of view) were prescribed for a standardized spatial region encompassing the palatine process region cranially to the cricoid cartilage caudally for all scans. T2w and T1w axial images with and without contrast were acquired using a fast spin-echo sequence (T2w: repetition time/echo time (TR/TE) = 3.6 s/100 ms, echo train length = 16; T1w: TR/TE = 600/7 ms, echo train length = 2). Thirty axial slices with a field of view of 25.6 cm and slab thickness of 12 cm were selected to cover the parotid glands, primary tumor, and metastasis-bearing cervical lymph nodes for ADC and IVIM parameter measurements. Acquisition parameters for IVIM-MRI were single-shot, spin-echo echo-planar imaging sequence, axial acquisition, TR = 3.6 s, TE = 80 ms, pixel size = 2 × 2 mm^2 in-plane, bandwidth = 1,950 Hz/pixel, slice thickness = 3.5 mm with a 0.5-mm gap, 30 contiguous slices, number of signal averages = 2~6 (2 averages for b-value < 200 s/mm^2; 4 averages for b-value ≥ 200 s/mm^2; 6 averages for b-value = 800 s/mm^2), and 128 × 128 matrix with parallel imaging factor 2 and chemical-shift-based fat suppression applied. A total of 12 b-values were acquired (0, 20, 40, 60, 80, 100, 120, 150, 200, 400, 600, and 800 s/mm^2) for each orthogonal diffusion direction.

Image Analysis

Regions of interest for the primary tumor and metastatic nodal mass were identified and drawn by two radiation oncologists (ASRM and CDF) and an MRI physicist (YD), based on T2w, T1w-Gd, and high-b-value (b = 800 s/mm^2) diffusion images. The IVIM parameters obtained for each lesion were calculated on a pixel-by-pixel basis and expressed as means for all voxels within the lesion volume of interest, using a method previously described by

Sumi et al (20,34) . IVIM parameters can be obtained by biexponential fitting of the diffusion-attenuated MRI signal intensity from multiple b-values as $S_b/S_0 = (1 - f) \cdot \exp(-bD) + f \cdot \exp[-b(D^* + D)]$, where S_b is the signal intensity in the pixel with diffusion gradient b, S_0 is the signal intensity in the pixel without a diffusion gradient, D is the true diffusion as reflected by pure molecular diffusion, f is the fractional perfusion related to microcirculation, and D^* is the pseudodiffusion coefficient related to perfusion. D was obtained by the simplified linear fit equation $S_b = S_0 \times \exp(-b \cdot D)$ using b-values ≥ 200 s/mm^2, whereas f and D^* were calculated by a non-linear least squares (NLLS) regression algorithm with 12 b-values ranging from 0 to 800 s/mm^2. In addition, ADC was calculated by a monoexponential fit of signal intensity (b = 0, 400, and 800 s/mm^2): $S_b = S_0 \times \exp(-b \cdot \text{ADC})$. All regression algorithms were implemented with ImageJ software (NIH, Bethesda, MD, USA) (34), allowing us to extract parametric maps representing D, D*, *f*, and ADC, fitted on a pixel-by-pixel basis. When the fits did not converge, the corresponding voxels were excluded from quantitative analysis.

Statistical Analysis

A mean and a standard deviation were calculated for each parameter at each interval scan. The nonparametric Mann-Whitney U test was used to assess differences in ADC and IVIM parameters between the CR group and the non CR group. Univariate logistic regression was used to evaluate the extent to which midtreatment changes in each imaging feature can be used to predict sites that would achieve CR. Partial effects were evaluated for significance using two-sided Wald tests. Bonferroni correction was used to control the familywise type I error rate at the 0.05 significance level, inducing the significance threshold of 0.025. Bayesian quadratic discriminant analysis (QDA) (35) was used to evaluate the extent to which midtreatment changes in these correlated imaging features predict sites that would achieve CR in multivariate analysis. Results for multivariate prediction model are reported for the best subset of predictors (ΔADC and ΔD), which were identified using stepwise backward model selection based on Akaike information criterion.(36) Parameters for each level of response assumed independent priors. The mean vectors assumed flat priors, while the covariance for each response level assumed an inverse Wishart prior with shape=2 and scale matrix estimated from the data as the maximizer of the marginal density (empirical Bayesian method). The prior probability of each response level was fixed at 0.5. Specificity, sensitivity, and accuracy were determined using a leave-one-site out cross-validation (LOOCV) strategy whereby each lesion's treatment response was predicted after training the Bayesian model using data from the other 59 lesions. Each site was assigned to the response level resulting in higher predicted probability. Receiver operating characteristic (ROC) curves were computed using the predicted response probabilities. The method of Delong et al(37) was used to calculate the 95% confidence interval for the area under the curve (AUC). The sample size of 59 lesions provides 80% power to detect an AUC of at least 0.69 at α=0.05 assuming that 19 lesions achieve CR. All analyses were executed with JMP Pro version 11 software (SAS Institute, Cary, NC) or statistical software R version 3.1.2. (R Development Core Team, http://www.r-project.org).

Results

Patients and Lesions

A total of 40 patients were eligible for study inclusion and provided study-specific informed consent. Six patients were excluded from final analysis because they withdrew from the imaging part of the study before midtreatment imaging, and three patients were excluded because of dental artifacts precluding signal assessment. MRI data were analyzed for the remaining 31 patients. Median age was 57 years (range, 44–78), with 29 men and 2 women. 16 patients (52%) were treated by intensity modulated radiotherapy and 15 (48%) were treated by intensity modulated proton therapy (IMPT). The majority of patients (78%) received Cisplatin chemotherapy concurrently with radiotherapy. Patient, disease, and treatment characteristics are summarized in Table 1. A total of 61 lesions (primary tumors and nodal metastases) were segmented. Two lesions were excluded: one primary tumor, due to echo-planar imaging-related severe geometric distortion, and one nodal lesion, due to poor signal-to-noise ratio out of rather posterior coil coverage leaving 59 lesions for analysis.

Midtreatment Response

Of the 29 primary tumors, 15 had a CR and 14 had a PR on midtreatment scans according to RECIST criteria. Of the 30 lymph node metastases, 4 had a CR, 22 had a PR, and 4 had stable disease on midtreatment scans. The median number of RT fractions received before the midtreatment scan was 17 (range, 15–26). Pretreatment ADC and D values for lesions that had a midtreatment CR (19 lesions) were significantly lower than those that did not have a CR ($(0.82 \pm 0.17) \times 10^{-3}$ mm^2/s vs. $(0.94 \pm 0.19) \times 10^{-3}$ mm^2/s, $P = .03$ for ADC, and $(0.69 \pm 0.12) \times 10^{-3}$ mm^2/s vs. $(0.82 \pm 0.16) \times 10^{-3}$ mm^2/s, $P = .003$ for D). Pretreatment D*, and *f* values for the CR lesions were not statistically different from those that did not have a CR as shown in Table 2.

Midtreatment ADC, D, and *f* values were significantly ($P < .0001$) increased compared to the pretreatment values for all lesions (Table 2). Midtreatment D* values, however, were not statistically different from pretreatment D* values. Lesions that had a CR were associated with significantly higher normalized ΔADC, ΔD, and Δ*f* values than non-CR lesions ($P < .0001$ for both ΔADC and ΔD and $P = .003$ for Δ*f*), while the study failed to yield evidence of a significant difference in ΔD* values between CR and non-CR lesions ($P = .6$). Fig. 2 shows boxplots of normalized delta values for all tested parameters in both CR and non-CR lesions. After stratification of lesions by primary tumor and nodal sites; primary tumors that achieved CR were associated with significantly higher normalized ΔADC, ΔD, and Δ*f* values than non-CR ($P < .0005$ for ΔADC, and $P = .01$ for both ΔD and Δ*f*), while ΔD* was insignificant ($P = .7$). While, nodes that achieved CR were associated with significantly higher normalized ΔADC and ΔD values than non-CR ($P < .0001$ for both), and insignificant ΔD* and Δ*f* ($P > .05$).

Additional, *post hoc* analysis of ΔADC, ΔD, ΔD* and Δ*f* changes as a function of radiotherapy technique (IMRT vs. IMPT), and as a function of various chemotherapy agents

(Cisplatin vs. others) revealed no statistically significant difference in parameters' Δ changes among the studied groups (all $P > .05$).

Fig. 3A provides a scatterplot of the imaging features. Significant associations were evident from logistic regression analysis. Each increase in normalized ΔADC of size 0.1 yielded a 1.65-fold increase in the odds of CR ($P < .00027$), each increase in normalized ΔD of size 0.1 yielded a 1.45-fold increase in the odds of CR ($P < .00024$), and each unit increase in Δ*f* yielded a 2.29-fold increase in the odds of CR ($P < .024$). Combined ΔD and ΔADC parameters yielded sensitivity=0.63, specificity=0.85, and accuracy=0.78 using Bayesian QDA for predicting CR under LOOCV. Fig. 3B presents the resulting posterior probability of CR as a function of normalized ΔADC and normalized ΔD. In addition, the Bayesian model yielded an AUC=0.87 (95% CI: 0.79, 0.96) for predicting the CR under LOOCV. The ROC curve is provided in Fig. 3C. Supplementary Fig. S1 shows a scatterplot depicting midtreatment changes in ΔD and Δ*f* for patients experiencing presence/absence of CR.

Fig. 4 shows representative pretreatment and midtreatment images of a primary base-of-tongue tumor that had a PR. The primary tumor had high signal intensity in T2w and T1w-Gd images and hyperintense signal intensity in the DW image (b = 800 s/mm^2). Pretreatment and midtreatment values in the primary tumor were, respectively, as follows: ADC, $(0.78 \pm 0.18) \times 10^{-3}$ and $(1.65 \pm 0.14) \times 10^{-3}$ mm^2/s; D, $(0.53 \pm 0.15) \times 10^{-3}$ and $(1.43 \pm 0.13) \times 10^{-3}$ mm^2/s; D*, $(2.6 \pm 3.1) \times 10^{-2}$ and $(2.3 \pm 0.3) \times 10^{-2}$ mm^2/s; *f*, 0.13 ± 0.17 and 0.12 ± 0.12 mm^2/s. Midtreatment signal decay in the primary tumor was faster than pretreatment signal decay.

Fig. 5 shows representative images from a patient (patient 5) with a midtreatment CR in the primary tumor (right tonsil) and a midtreatment PR in a lymph node metastasis. Both the residual tumor and the node showed significant midtreatment changes in contrast in the region of interest. Pretreatment and midtreatment values for the primary tumor were, respectively, as follows: ADC, $(0.91 \pm 0.09) \times 10^{-3}$ and $(1.71 \pm 0.14) \times 10^{-3}$ mm^2/s; D, $(0.63 \pm 0.17) \times 10^{-3}$ and $(1.57 \pm 0.09) \times 10^{-3}$ mm^2/s; D*, $(1.4 \pm 2.2) \times 10^{-2}$ and $(4.2 \pm 3.3) \times 10^{-2}$ mm^2/s; *f*, 0.21 ± 0.09 and 0.26 ± 0.13 mm^2/s. For the nodal lesion, pretreatment and midtreatment values were, respectively, as follows: metastatic node, ADC, $(0.98 \pm 0.22) \times 10^{-3}$ and $2.04 \pm 0.21 \times 10^{-3}$ mm^2/s; D, $(0.88 \pm 0.26) \times 10^{-3}$ and $(1.71 \pm 0.26) \times 10^{-3}$ mm^2/s; D*, $(2.2 \pm 2.3) \times$ and $(2.0 \pm 1.7) \times 10^{-2}$ mm^2/s; *f*, 0.11 ± 0.10, and 0.28 ± 0.14 mm^2/s. Midtreatment signal decay in the primary tumor was significantly faster than pretreatment signal decay, but the difference in the rate of signal decay for the node between the two time points was relatively small.

Post-treatment Response

At post-treatment assessment 100 % of non-CR primary tumor lesions eventually achieved CR while 26 (87%) of non-CR nodal lesions had CR. The remaining 4 (13%) nodal lesions with post-treatment PR were treated by salvage neck dissection and revealed no viable residual cancer cells in pathologic examination.

Discussion

Our data showed that a lower pretreatment ADC and D values was associated with early radiologic CR, while the pretreatment perfusion-related parameters were not. Additionally, lesions that had a midtreatment CR had significantly higher ΔADC, ΔD, and Δf values than did lesions that did not have a CR. A model combining normalized ΔADC and ΔD can accurately discriminate between patients with a midtreatment CR from patients without a midtreatment CR which can be useful for therapy response monitoring in HPV+ population and will help to identify patients for potential dose de-escalation in future studies.

Previous studies showed that tumor regression during radiotherapy is an independent predictive factor of local control in several malignancies (38,39) and also for head and neck cancer patients.(40) Recently tumor regression rate at midtreatment was shown to predict locoregional control in oropharyngeal cancer patients.(29) While we plan to confirm whether local/regional control is, over the long-term, predicted by IVIM as a treatment response bio-indicator, a goal of the current study is to determine whether patients might be selected for adaptive re-planning applications. Consequently, since almost all patients' lesions had complete response at post-therapy follow-up, we contend that, for a subset of patients, we may actually be over-treating with current doses prescribed to HPV+ oropharyngeal cancer patients.

Until recent years, there has been limited evidence for clinical feasibility of IVIM MRI for head and neck cancer, even though IVIM was initially described more than 25 years ago (11). IVIM imaging, especially in oropharyngeal cancer, faces many technical challenges, including head and neck motion-induced artifacts (e.g. swallowing, neck rotation, tongue movement, etc.) during a comparatively lengthy scan, as well as susceptibility artifacts that may compromise IVIM data quality. In previous efforts, IVIM imaging of in the head and neck was limited by a heterogeneity of tumor populations, as most series included mixed tumor subsites, histologies, and HPV statuses (20–24,27). In this preliminary study, IVIM data were prospectively collected from a homogenous cohort of HPV+ oropharyngeal SCC patients in an ongoing clinical trial (32). MR images were acquired using our previously standardized radiotherapy immobilization setup, which ameliorated many of the motion-associated artifacts seen in previous MRI efforts for advanced head and neck cancer(33). Moreover, it has been recognized that for accurate model fitting of IVIM MRI data, sufficiently high signal to noise ratio (SNR) has to be achieved in the acquired data (41,42). For this reason, we applied flex coils centered in primary tumor region with multiple averages to ensure adequate SNR achieved for IVIM parameter estimation. However, we still consider that applying the widely used NLLS fitting results in a relative variation of D^* and f measurements, especially in midtreatment scans due to the relatively lower SNR. Therefore, other approaches which can provide more robust estimation of the IVIM parameters at lower SNR are required after proper validation in future investigations (43).

Recently, Lai et al (22) reported that IVIM MRI might be feasible and useful in differentiating nasopharyngeal carcinoma and postchemoradiation fibrosis. More recently, Hauser et al applied the IVIM model to HNSCC primary tumors (21) and lymph node metastases (44) and reported that IVIM MRI may be helpful for predicting poor treatment

response in patients with HNSCC. Pretreatment ADC was shown by Kim et al (9) to be predictive of CR in a sample of mixed HNSCC sites, matching our findings that pretreatment ADC was associated with midtreatment CR. Pretreatment ADC was also shown to be correlated with local failure in a retrospectively analyzed cohort of 38 HNSCCs (45). A higher ΔADC at week 1 of treatment was shown by Kim et al to be predictive of CR (in agreement with our midtreatment results), with AUC of 0.88, 86% sensitivity, and 83% specificity(9). Additionally, high ΔADCs at weeks 2 and 4 of treatment were predictive of improved 2-year locoregional control, as reported by Vandecaveye et al (10). In a series of 22 locally advanced HNSCCs, Hauser et al (21) recently reported that relatively high pretreatment *f* and ADC values were associated with poor clinical outcome at minimum follow-up of 7.5 months.

As with any pilot technology development protocol, caveats apply. First, the number of patients was limited. As patients accrue to the parent study, however, we plan to acquire more images and report actuarial outcomes (e.g. local control, locoregional control, and overall survival) as a function of biomarker kinetics with a larger sample. Second, we did not test the short-term repeatability/reproducibility of IVIM parameters, so as not to inconvenience the patients. However, efforts are under way to perform “zero-change” assessments to validate our measurements in another pretherapy protocol. Finally, we did not address geometric distortion, which may be severe in regions with air-tissue transitions (e.g. the base of the tongue), and eddy current effects, which may limit adaptive replanning in radiotherapy (46–48). Effective correction methods and other imaging techniques will be tested and validated in our future studies.

Despite the limitations, this study represents, to our knowledge, the first assessment of the feasibility of characterizing pretreatment and midtreatment tumor and nodal IVIM-MRI temporal kinetics in a prospective cohort of chemoradiotherapy patients with HPV+ oropharyngeal cancer. Furthermore, our data suggest that IVIM parameters can potentially identify at actionable time points tumors likely to rapidly respond to chemoradiotherapy. Such potentially predictive IVIM parameters include pretreatment D and ADC, which could be used in stratifying patients for dose adaptation at simulation, and midtreatment ΔADC and ΔD which could serve as interval markers for plan adaptation midtherapy. Our findings will need to be confirmed in prospective studies with large data sets.

In conclusion, the present study showed that noninvasive IVIM MRI is feasible and potentially useful for predicting and assessing early responses of HPV+ oropharyngeal SCC to chemoradiotherapy. IVIM data may have translational applications in adaptive treatment planning, prediction of outcome, and monitoring of treatment response.

Supplementary Material

Refer to Web version on PubMed Central for supplementary material.

Acknowledgments

We thank Paul Wisdom and the rest of the machine shop team in the Department of Radiation Oncology, MD Anderson Cancer Center, for their assistance in constructing the MR-compatible immobilization platform. We also

thank the Imaging Physics Medical Imaging Technologist team of Jerrell Jones, Clemente Logronio Jr., Brandy Reed, Michelle Underwood, and David Timothy Evans for executing all studies performed at the Center for Advanced Biomedical Imaging and Dr. Ken-Pin Hwang from General Electric Healthcare Technologies for great efforts in acquiring MR scans of patients.

Abbreviations

IVIM	Intravoxel incoherent motion
HPV+	human papillomavirus-associated
HNSCC	head and neck squamous cell carcinoma
DWI	diffusion-weighted imaging
ADC	apparent diffusion coefficient
D*	pseudo-diffusion coefficient
f	perfusion fraction
D	pure diffusion coefficient
RECIST criteria	Response Evaluation Criteria in Solid Tumors
IRB	institutional Review Board
AJCC	American Joint Committee on Cancer
ECOG	Eastern Cooperative Oncology Group
PR	partial response
CR	complete response
QDA	Bayesian quadratic discriminant analysis
LOOCV	a leave-one-site out cross-validation
ROC	receiver operating characteristic
AUC	area under the curve

References

1. Dawson LA, Anzai Y, Marsh L, Martel MK, Paulino A, Ship JA, Eisbruch A. Patterns of local-regional recurrence following parotid-sparing conformal and segmental intensity-modulated radiotherapy for head and neck cancer. International journal of radiation oncology, biology, physics. 2000; 46(5):1117–1126.
2. Chao KS, Ozyigit G, Tran BN, Cengiz M, Dempsey JF, Low DA. Patterns of failure in patients receiving definitive and postoperative IMRT for head-and-neck cancer. International journal of radiation oncology, biology, physics. 2003; 55(2):312–321.
3. Bentzen SM, Gregoire V. Molecular Imaging-Based Dose Painting: A Novel Paradigm for Radiation Therapy Prescription. Seminars in radiation oncology. 2011; 21(2):101–110. [PubMed: 21356478]
4. Dirix P, Vandecaveye V, De Keyzer F, Stroobants S, Hermans R, Nuyts S. Dose Painting in Radiotherapy for Head and Neck Squamous Cell Carcinoma: Value of Repeated Functional Imaging with F-18-FDG PET, F-18-Fluoromisonidazole PET, Diffusion-Weighted MRI, and Dynamic Contrast-Enhanced MRI. Journal of Nuclear Medicine. 2009; 50(7):1020–1027. [PubMed: 19525447]

5. Johansen R, Jensen LR, Rydand J, Goa PE, Kvistad KA, Bathen TF, Axelson DE, Lundgren S, Gribbestad IS. Predicting Survival and Early Clinical Response to Primary Chemotherapy for Patients With Locally Advanced Breast Cancer Using DCE-MRI. J Magn Reson Imaging. 2009; 29(6):1300–1307. [PubMed: 19472387]
6. Patterson DM, Padhani AR, Collins DJ. Technology Insight: water diffusion MRI - a potential new biomarker of response to cancer therapy. Nat Clin Pract Oncol. 2008; 5(4):220–233. [PubMed: 18301415]
7. Thoeny HC, Ross BD. Predicting and monitoring cancer treatment response with diffusion-weighted MRI. Journal of magnetic resonance imaging : JMRI. 2010; 32(1):2–16. [PubMed: 20575076]
8. Vandecaveye V, De Keyzer F, Nuyts S, Deraedt K, Dirix P, Hamaekers P, Vander Poorten V, Delaere P, Hermans R. Detection of head and neck squamous cell carcinoma with diffusion weighted MRI after (chemo)radiotherapy: correlation between radiologic and histopathologic findings. International journal of radiation oncology, biology, physics. 2007; 67(4):960–971.
9. Kim S, Loevner L, Quon H, Sherman E, Weinstein G, Kilger A, Poptani H. Diffusion-weighted magnetic resonance imaging for predicting and detecting early response to chemoradiation therapy of squamous cell carcinomas of the head and neck. Clin Cancer Res. 2009; 15(3):986–994. [PubMed: 19188170]
10. Vandecaveye V, Dirix P, De Keyzer F, de Beeck KO, Vander Poorten V, Roebben I, Nuyts S, Hermans R. Predictive value of diffusion-weighted magnetic resonance imaging during chemoradiotherapy for head and neck squamous cell carcinoma. European radiology. 2010; 20(7): 1703–1714. [PubMed: 20179939]
11. Le Bihan D, Breton E, Lallemand D, Aubin ML, Vignaud J, Laval-Jeantet M. Separation of diffusion and perfusion in intravoxel incoherent motion MR imaging. Radiology. 1988; 168(2): 497–505. [PubMed: 3393671]
12. Le Bihan D. Intravoxel incoherent motion perfusion MR imaging: a wake-up call. Radiology. 2008; 249(3):748–752. [PubMed: 19011179]
13. Sigmund EE, Cho GY, Kim S, Finn M, Moccaldi M, Jensen JH, Sodickson DK, Goldberg JD, Formenti S, Moy L. Intravoxel incoherent motion imaging of tumor microenvironment in locally advanced breast cancer. Magn Reson Med. 2011; 65(5):1437–1447. [PubMed: 21287591]
14. Kim T, Kim SG. Quantification of cerebral arterial blood volume using arterial spin labeling with intravoxel incoherent motion-sensitive gradients. Magnetic resonance in medicine : official journal of the Society of Magnetic Resonance in Medicine/Society of Magnetic Resonance in Medicine. 2006; 55(5):1047–1057.
15. Federau C, Maeder P, O'Brien K, Browaeys P, Meuli R, Hagmann P. Quantitative measurement of brain perfusion with intravoxel incoherent motion MR imaging. Radiology. 2012; 265(3):874–881. [PubMed: 23074258]
16. Luciani A, Vignaud A, Cavet M, Nhieu JT, Mallat A, Ruel L, Laurent A, Deux JF, Brugieres P, Rahmouni A. Liver cirrhosis: intravoxel incoherent motion MR imaging--pilot study. Radiology. 2008; 249(3):891–899. [PubMed: 19011186]
17. Chandarana H, Kang SK, Wong S, Rusinek H, Zhang JL, Arizono S, Huang WC, Melamed J, Babb JS, Suan EF, Lee VS, Sigmund EE. Diffusion-weighted intravoxel incoherent motion imaging of renal tumors with histopathologic correlation. Investigative radiology. 2012; 47(12): 688–696. [PubMed: 22996315]
18. Lemke A, Laun FB, Klauss M, Re TJ, Simon D, Delorme S, Schad LR, Stieltjes B. Differentiation of pancreas carcinoma from healthy pancreatic tissue using multiple b-values: comparison of apparent diffusion coefficient and intravoxel incoherent motion derived parameters. Investigative radiology. 2009; 44(12):769–775. [PubMed: 19838121]
19. Dopfert J, Lemke A, Weidner A, Schad LR. Investigation of prostate cancer using diffusion-weighted intravoxel incoherent motion imaging. Magnetic resonance imaging. 2011; 29(8):1053–1058. [PubMed: 21855241]
20. Sumi M, Van Cauteren M, Sumi T, Obara M, Ichikawa Y, Nakamura T. Salivary gland tumors: use of intravoxel incoherent motion MR imaging for assessment of diffusion and perfusion for the differentiation of benign from malignant tumors. Radiology. 2012; 263(3):770–777. [PubMed: 22447854]

21. Hauser T, Essig M, Jensen A, Gerigk L, Laun FB, Munter M, Simon D, Stieltjes B. Characterization and therapy monitoring of head and neck carcinomas using diffusion-imaging-based intravoxel incoherent motion parameters-preliminary results. Neuroradiology. 2013; 55(5): 527–536. [PubMed: 23417120]
22. Lai V, Li X, Lee VH, Lam KO, Chan Q, Khong PL. Intravoxel incoherent motion MR imaging: comparison of diffusion and perfusion characteristics between nasopharyngeal carcinoma and post-chemoradiation fibrosis. European radiology. 2013; 23(10):2793–2801. [PubMed: 23722897]
23. Lu Y, Jansen JF, Stambuk HE, Gupta G, Lee N, Gonen M, Moreira A, Mazaheri Y, Patel SG, Deasy JO, Shah JP, Shukla-Dave A. Comparing primary tumors and metastatic nodes in head and neck cancer using intravoxel incoherent motion imaging: a preliminary experience. Journal of computer assisted tomography. 2013; 37(3):346–352. [PubMed: 23674004]
24. Marzi S, Piludu F, Vidiri A. Assessment of diffusion parameters by intravoxel incoherent motion MRI in head and neck squamous cell carcinoma. NMR in biomedicine. 2013; 26(12):1806–1814. [PubMed: 23996455]
25. Ang KK, Harris J, Wheeler R, Weber R, Rosenthal DI, Nguyen-Tan PF, Westra WH, Chung CH, Jordan RC, Lu C, Kim H, Axelrod R, Silverman CC, Redmond KP, Gillison ML. Human papillomavirus and survival of patients with oropharyngeal cancer. The New England journal of medicine. 2010; 363(1):24–35. [PubMed: 20530316]
26. Hong AM, Dobbins TA, Lee CS, Jones D, Harnett GB, Armstrong BK, Clark JR, Milross CG, Kim J, O'Brien CJ, Rose BR. Human papillomavirus predicts outcome in oropharyngeal cancer in patients treated primarily with surgery or radiation therapy. British journal of cancer. 2010; 103(10):1510–1517. [PubMed: 20959828]
27. Hauser T, Essig M, Jensen A, Laun FB, Munter M, Maier-Hein KH, Stieltjes B. Prediction of treatment response in head and neck carcinomas using IVIM-DWI: Evaluation of lymph node metastasis. Eur J Radiol. 2014; 83(5):783–787. [PubMed: 24631600]
28. Bhatia KSS, King AD, Yu KH, Vlantis AC, Tse GM, Mo FK, Ahuja AT. Does primary tumour volumetry performed early in the course of definitive concomitant chemoradiotherapy for head and neck squamous cell carcinoma improve prediction of primary site outcome? Brit J Radiol. 2010; 83(995):964–970. [PubMed: 20965907]
29. Lee H, Ahn YC, Oh D, Nam H, Kim YI, Park SY. Tumor volume reduction rate measured during adaptive definitive radiation therapy as a potential prognosticator of locoregional control in patients with oropharyngeal cancer. Head Neck-J Sci Spec. 2014; 36(4):499–504.
30. Hermans R. Head and neck cancer: how imaging predicts treatment outcome. Cancer imaging : the official publication of the International Cancer Imaging Society. 2006; 6:S145–153. [PubMed: 17114069]
31. Eisenhauer EA, Therasse P, Bogaerts J, Schwartz LH, Sargent D, Ford R, Dancey J, Arbuck S, Gwyther S, Mooney M, Rubinstein L, Shankar L, Dodd L, Kaplan R, Lacombe D, Verweij J. New response evaluation criteria in solid tumours: Revised RECIST guideline (version 1. 1). European journal of cancer. 2009; 45(2):228–247. [PubMed: 19097774]
32. Frank, SJ. ClinicalTrials.gov Identifier: NCT01893307. M.D. Anderson Cancer Center; Intensity-Modulated Proton Beam Therapy (IMPT) Versus Intensity-Modulated Photon Therapy (IMRT). https://clinicaltrials.gov/ct2/show/NCT01893307?term=head+neck+frank&rank=2 [last access 6.13.2014]
33. Ding Y, Mohamed AS, Yang J, Colen RR, Frank SJ, Wang J, Wassal EY, Wang W, Kantor ME, Balter PA, Rosenthal DI, Lai SY, Hazle JD, Fuller CD. Prospective observer and software-based assessment of magnetic resonance imaging quality in head and neck cancer: Should standard positioning and immobilization be required for radiation therapy applications? Pract Radiat Oncol. 2014
34. Sumi M, Nakamura T. Head and neck tumors: assessment of perfusion-related parameters and diffusion coefficients based on the intravoxel incoherent motion model. AJNR American journal of neuroradiology. 2013; 34(2):410–416. [PubMed: 22859281]
35. Srivastava S, Gupta MR, Frigyik BA. Bayesian quadratic discriminant analysis. J Mach Learn Res. 2007; 8:1277–1305.
36. Akaike H. New Look at Statistical-Model Identification. Ieee T Automat Contr. 1974; Ac19(6): 716–723.

37. DeLong ER, DeLong DM, Clarke-Pearson DL. Comparing the areas under two or more correlated receiver operating characteristic curves: a nonparametric approach. Biometrics. 1988; 44(3):837–845. [PubMed: 3203132]
38. Nam H, Park W, Huh SJ, Bae DS, Kim BG, Lee JH, Lee JW, Lim DH, Han Y, Park HC, Ahn YC. The prognostic significance of tumor volume regression during radiotherapy and concurrent chemoradiotherapy for cervical cancer using MRI. Gynecol Oncol. 2007; 107(2):320–325. [PubMed: 17675222]
39. Bral S, De Ridder M, Duchateau M, Gevaert T, Engels B, Schallier D, Storme G. Daily Megavoltage Computed Tomography in Lung Cancer Radiotherapy: Correlation between Volumetric Changes and Local Outcome. Int J Radiat Oncol. 2011; 80(5):1338–1342.
40. Jaulerry C, Dubray B, Brunin F, Rodriguez J, Point D, Blaszka B, Asselain B, Mosseri V, Brugere J, Cosset JM. Prognostic value of tumor regression during radiotherapy for head and neck cancer: a prospective study. International journal of radiation oncology, biology, physics. 1995; 33(2): 271–279.
41. Le Bihan D, Turner R, Moonen CT, Pekar J. Imaging of diffusion and microcirculation with gradient sensitization: design, strategy, and significance. Journal of magnetic resonance imaging : JMRI. 1991; 1(1):7–28. [PubMed: 1802133]
42. Pekar J, Moonen CT, van Zijl PC. On the precision of diffusion/perfusion imaging by gradient sensitization. Magnetic resonance in medicine : official journal of the Society of Magnetic Resonance in Medicine/Society of Magnetic Resonance in Medicine. 1992; 23(1):122–129.
43. Neil JJ, Bretthorst GL. On the use of Bayesian probability theory for analysis of exponential decay data: an example taken from intravoxel incoherent motion experiments. Magnetic resonance in medicine : official journal of the Society of Magnetic Resonance in Medicine/Society of Magnetic Resonance in Medicine. 1993; 29(5):642–647.
44. Hauser T, Essig M, Jensen A, Laun FB, Munter M, Maier-Hein KH, Stieltjes B. Prediction of treatment response in head and neck carcinomas using IVIM-DWI: Evaluation of lymph node metastasis. European journal of radiology. 2014; 83(5):783–787. [PubMed: 24631600]
45. Hatakenaka M, Nakamura K, Yabuuchi H, Shioyama Y, Matsuo Y, Ohnishi K, Sunami S, Kamitani T, Setoguchi T, Yoshiura T, Nakashima T, Nishikawa K, Honda H. Pretreatment apparent diffusion coefficient of the primary lesion correlates with local failure in head-and-neck cancer treated with chemoradiotherapy or radiotherapy. International journal of radiation oncology, biology, physics. 2011; 81(2):339–345.
46. Schakel T, Hoogduin JM, Terhaard CH, Philippens ME. Diffusion weighted MRI in head-and-neck cancer: Geometrical accuracy. Radiotherapy and oncology : journal of the European Society for Therapeutic Radiology and Oncology. 2013
47. Pipe JG, Farthing VG, Forbes KP. Multishot diffusion-weighted FSE using PROPELLER MRI. Magnetic resonance in medicine : official journal of the Society of Magnetic Resonance in Medicine/Society of Magnetic Resonance in Medicine. 2002; 47(1):42–52.
48. Sakamoto J, Imaizumi A, Sasaki Y, Kamio T, Wakoh M, Otonari-Yamamoto M, Sano T. Comparison of accuracy of intravoxel incoherent motion and apparent diffusion coefficient techniques for predicting malignancy of head and neck tumors using half-Fourier single-shot turbo spin-echo diffusion-weighted imaging. Magnetic resonance imaging. 2014; 32(7):860–866. [PubMed: 24832359]

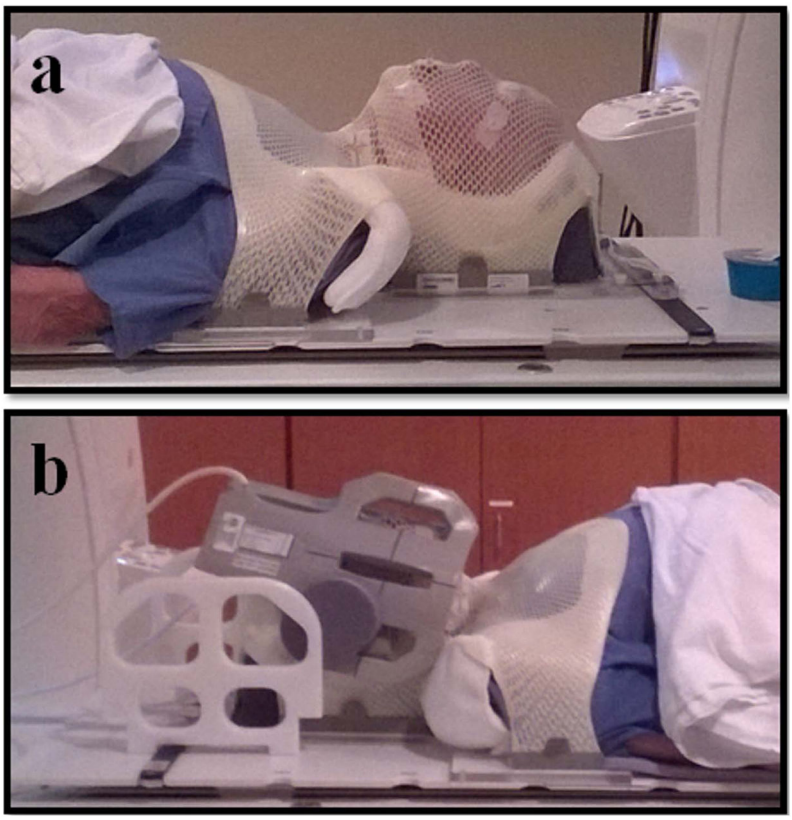

Fig. 1.
Patient setup used for imaging. (a) Klarity immobilization devices; (b) six-channel flex coils.

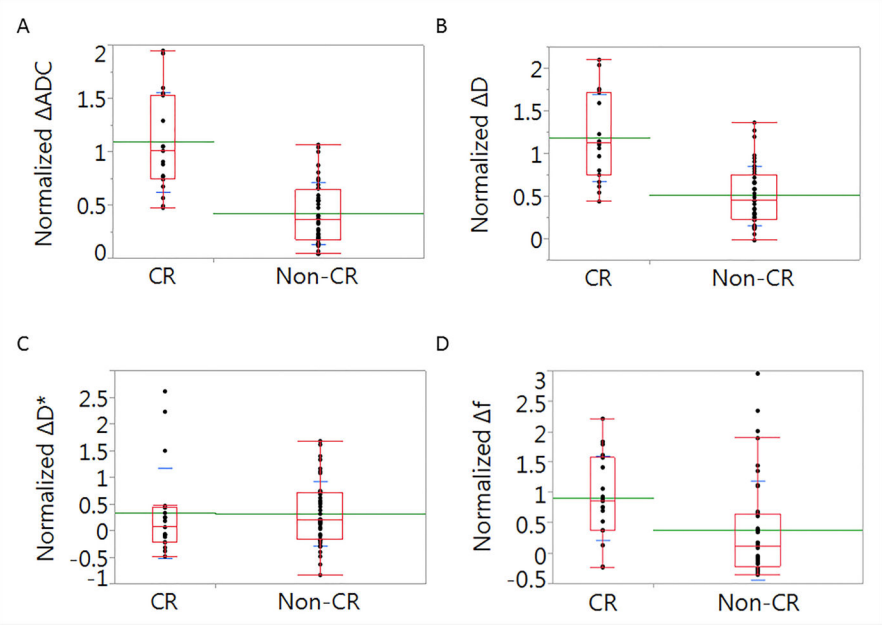

Fig. 2.

A box-plot depecting the differences between complete response (CR) and non-CR lesions in terms of normalized ΔADC (A), ΔD (B), ΔD* (C), and Δ*f* (D).

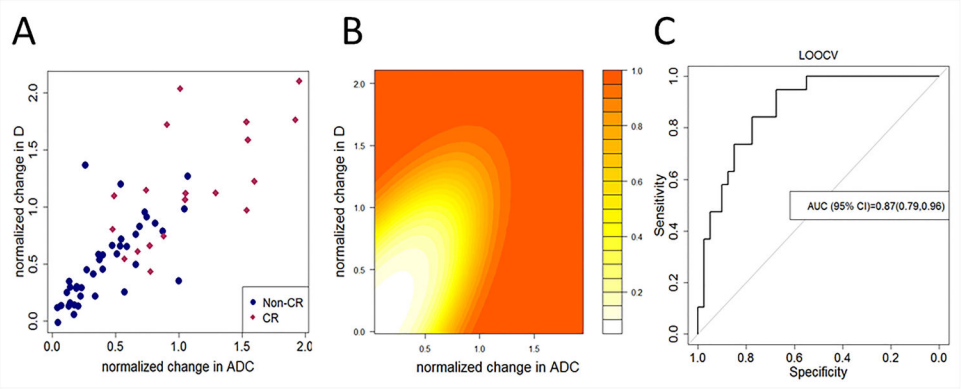

Fig. 3.

(A) shows a scatterplot depicting mid-therapy changes in ΔADC and ΔD for patients experiencing presence/absence of complete response (CR). (B) shows a Contour plot depicting the posterior probability of observing complete response as a function of mid-therapy changes in ΔADC and ΔD obtained from analysis using Bayesian QDA. (C) shows a Receiver operating characteristics curve obtained from the Bayesian model for predicting complete response using mid-therapy changes in ΔADC and ΔD using leave-one-out cross-validation. Combined the parameters attained an AUC=0.87 (95% CI: 0.79, 0.96) with sensitivity=0.63, specificity=0.85, and accuracy=0.78.

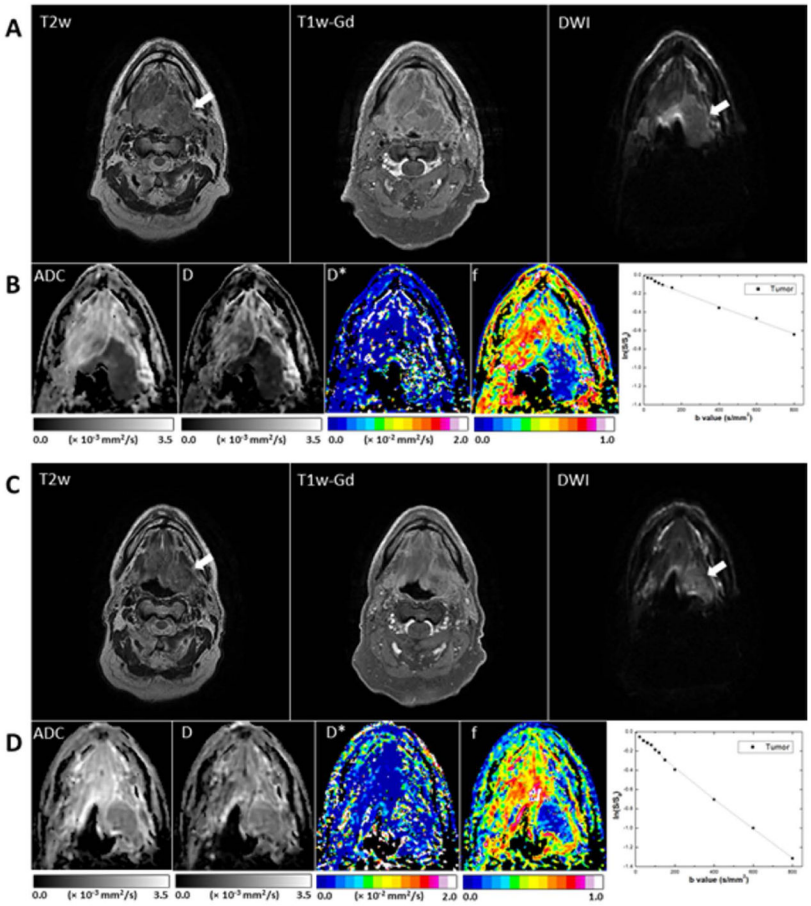

Fig. 4.

Representative MR images of a tumor that had a midtreatment PR (patient 16, a 55-year-old man). (A, B) Pretreatment scans; (C, D) midtreatment scans. The T2w, T1w-Gd, and DW (b = 800 mm/s^2) images (A, C) were windowed to have similar image contrast, whereas ADC and IVIM parametric maps (B, D) were scaled according to the scale bars shown below the images (the scales used for midtreatment images were the same as those used for preatment images). The primary mass is indicated by arrows. Logarithmic plots of biexponential signal decay in the primary tumor are shown on the right in panels B and D.

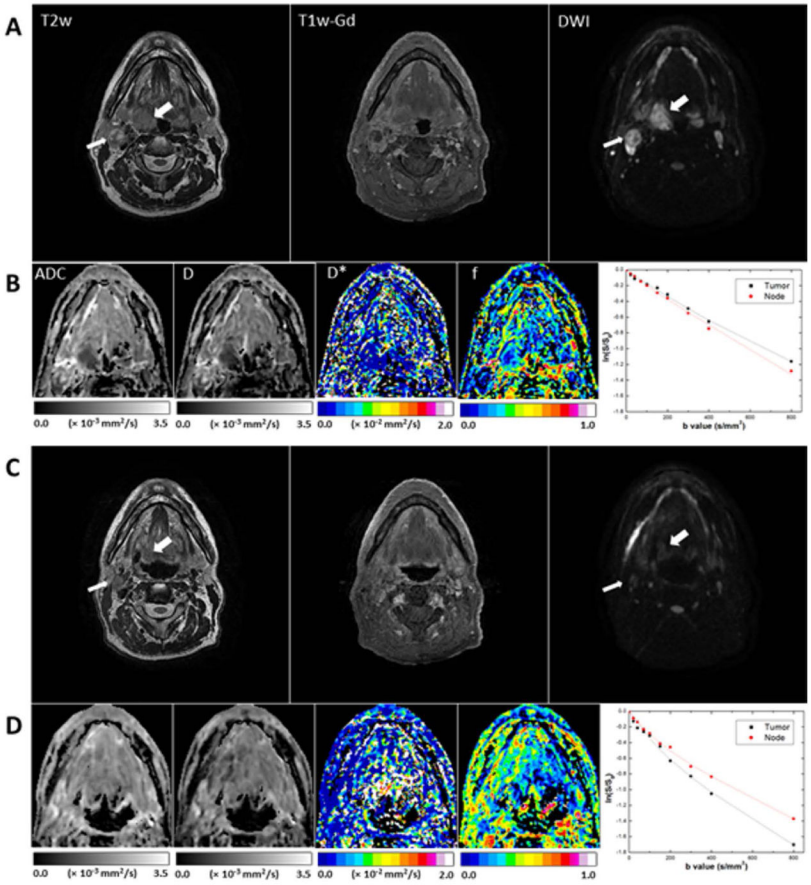

Fig. 5.

Representative MR images of a tumor (right tonsil; thick arrows) that had a midtreatment CR and a lymph node metastasis (thin arrows) that had a midtreatment PR (patient 5, a 60-year-old man). (A, B) Pretreatment scans; (C, D) midtreatment scans. The T2w, T1w-Gd, and DWI ($b = 800$ mm/s^2) images (A, C) were windowed to have similar image contrast, whereas ADC and IVIM parameter maps (B, D) were scaled according to the scale bars shown below the images (the scales used for midtreatment images were the same as those used for preatment images). Logarithmic plots of biexponential signal decay in the primary tumor and nodal metastasis are shown on the right in panels B and D.

Table 1

Characteristics of patients, tumors, and treatments

Characteristic	No. of patients (%)
Sex	
Female	2 (6)
Male	29 (94)
Age	
Median (range)	57 (44–78)
T stage (T)	
T1	1 (3)
T2	14 (45)
T3	8 (26)
T4	8 (26)
Nodal stage (N)	
N0	1 (3)
N1	3 (10)
N2a	2 (6)
N2b	13 (42)
N2c	12 (39)
N3	0 (0)
AJCC stage	
III	4 (13)
IVa	27 (87)
Smoking History at Diagnosis	
Never smoker	15 (48)
Current smoker	16 (52)
Disease sub-site	
Tonsil	16 (52)
Base of tongue	15 (48)
Total Radiation Dose	70 Gy
No. of Fractions Received	33
Radiation technique	
IMRT	16 (52)
IMPT	15 (48)
Chemotherapy	
Cetuximab	5 (16)
Carboplatin	1 (3)

Characteristic	No. of patients (%)
Cisplatin	24 (78)
Docetaxel	1 (3)

Note.—IMPT = intensity-modulated proton therapy, IMRT = intensity-modulated photon therapy.

Table 2

Pretreatment and midtreatment IVIM parameters

Midtreatment assessment	ADC (mm^2/s, $\times10^{-3}$)		D* (mm^2/s, $\times10^{-2}$)		D (mm^2/s, $\times10^{-3}$)		*f* (mm^2/s)	
	Pre-Tx	**Mid-Tx**	**Pre-Tx**	**Mid-Tx**	**Pre-Tx**	**Mid-Tx**	**Pre-Tx**	**Mid-Tx**
CR (n = 19)	0.83 ± 0.17	1.7 ± 0.33	3.0 ± 1.2	3.4 ± 0.12	0.69 ± 0.13	1.5 ± 0.27	0.14 ± 0.05	0.25 ± 0.10
Non-CR (n = 40)	0.94 ± 0.19†	1.3 ± 0.30	3.0 ± 1.4	3.5 ± 0.13	0.82 ± 0.15†	1.2 ± 0.29	0.13 ± 0.06	0.16 ± 0.08
Total (n = 59)	0.9 ± 0.19	1.4 ± 0.35‡	3.0 ± 1.3	3.5 ± 1.2	0.78 ± 0.16	1.3 ± 0.31‡	0.13 ± 0.05	0.19 ± 0.1‡

Note.—Tx = treatment, CR = complete response. The data are means with standard deviations.

†*Significant P* = .003 for pre-Tx ADC and D values in the CR group vs. the non-CR.

‡*Significant P* < .0001 for mid-Tx ADC, D, and *f* parameters increase vs. the pre-Tx values.